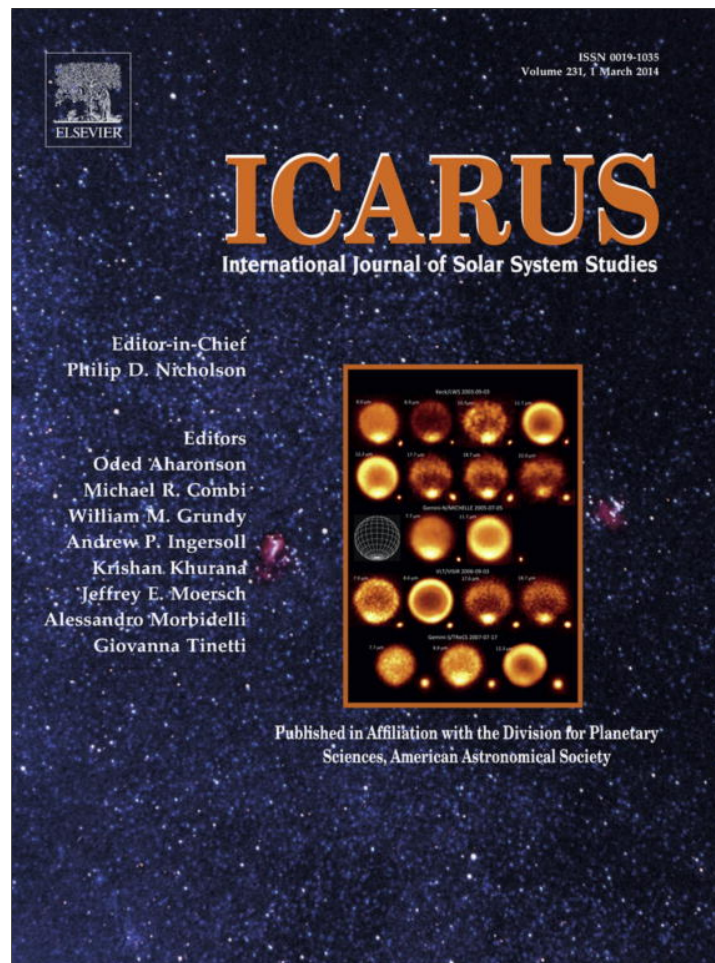


Provided for non-commercial research and education use.
Not for reproduction, distribution or commercial use.



This article appeared in a journal published by Elsevier. The attached copy is furnished to the author for internal non-commercial research and education use, including for instruction at the authors institution and sharing with colleagues.

Other uses, including reproduction and distribution, or selling or licensing copies, or posting to personal, institutional or third party websites are prohibited.

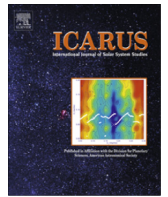
In most cases authors are permitted to post their version of the article (e.g. in Word or Tex form) to their personal website or institutional repository. Authors requiring further information regarding Elsevier's archiving and manuscript policies are encouraged to visit:

<http://www.elsevier.com/authorsrights>



Contents lists available at ScienceDirect

Icarus

journal homepage: www.elsevier.com/locate/icarus

The meteoroid fluence at Mars due to Comet C/2013 A1 (Siding Spring)



Althea V. Moorhead^{a,*}, Paul A. Wiegert^b, William J. Cooke^c

^a Geocent LLC, Jacobs ESSSA Group, Marshall Space Flight Center, Huntsville, AL 35812, United States

^b Department of Physics and Astronomy, The University of Western Ontario, London N6A3K7, Canada

^c NASA Meteoroid Environment Office, Marshall Space Flight Center, Huntsville, AL 35812, United States

ARTICLE INFO

Article history:

Received 29 August 2013

Revised 31 October 2013

Accepted 21 November 2013

Available online 1 December 2013

Keywords:

Comets, dust

Meteors

Mars

ABSTRACT

Long-period Comet C/2013 A1 (Siding Spring) will experience a close encounter with Mars on 2014 October 19. As of 2013 October 21, the distance of closest approach between the two is projected to be between 89,000 km and 173,000 km, with a nominal value of 131,000 km. Thus, a collision between the comet and the planet has been ruled out, but the comet's coma may very well envelop Mars and its man-made satellites. We present a simple analytic model of the dust component of cometary comae that describes the spatial distribution of cometary dust and meteoroids and their size distribution. We find that this model successfully reproduces, to within an order of magnitude, particle fluxes measured by spacecraft *Giotto* in the coma of 1P/Halley and by spacecraft *Stardust* in the coma of 81P/Wild 2. We apply our analytic model to C/2013 A1 (Siding Spring) and compute the expected total fluence of potentially damaging particles at Mars at the time of closest approach between the two bodies; we obtain a nominal fluence of 0.15 particles per square meter. We conduct numerical simulations of particle ejection from the comet's nucleus and compare the resulting spatial distribution with that of our analytic model, and conclude that our spherically symmetric analytic model is adequate for order-of-magnitude fluence estimates.

© 2013 Elsevier Inc. All rights reserved.

1. Introduction

Comet C/2013 A1 (Siding Spring) was discovered by astronomer Rob McNaught at Siding Spring observatory; using additional observations and predisccovery images from the Catalina Sky Survey, the comet was determined to be in a nearly parabolic orbit (McNaught et al., 2013). As of 2013 October 21, the JPL Small-Body Database classifies the orbit as hyperbolic for recent epochs but with an eccentricity of 0.99996 (relative to the Solar System barycenter) before entering the Solar System.¹

Siding Spring is notable in that it is projected to have a close encounter with Mars on 2014 October 19 at 18:34 ± 9 (TDB; Barycentric Dynamical Time). A collision between the comet and the planet has been ruled out and the close approach distance is currently estimated at 131,000 km, with a minimum of 89,000 km and a maximum of 173,000 km. Furthermore, Siding Spring shows activity in the earliest predisccovery images, dating back to 2012 October 4 when the comet was at a heliocentric distance of 7.2 au. Thus, by the time the comet encounters Mars it will have been producing dust and meteoroids for at least 2 years; as a

result, we expect the comet to have a sizable cometary coma capable of engulfing Mars.

Mars has three operational manmade satellites in orbit: NASA's Mars Reconnaissance Orbiter, NASA's Mars Odyssey, and ESA's Mars Express. One additional satellite, NASA's MAVEN (Mars Atmosphere and Volatile EvolutionN), is scheduled to arrive at Mars roughly one month prior to the Siding Spring close approach.² By virtue of their proximity to Mars, all four spacecraft will pass within 140,000 km of the comet. Hence, characterizing the dust environment is crucial for assessing the risk posed to these satellites by meteoroids in the comet's coma. During its flyby of 1P/Halley, the *Giotto* spacecraft detected particles at cometocentric distances as large as 287,000 km (McDonnell et al., 1987), which is twice the close approach distance between Siding Spring and Mars.

In this analysis, we compute the total fluence of dust particles 4.19×10^{-6} g or larger along a straight trajectory (i.e., a chord) through the spherical coma. We select this mass threshold because it is near the 10^{-6} g mass at which particles are generally considered potentially damaging (McNamara et al., 2004) and because, for a density of 1 g/cc, it corresponds to a spherical grain with a radius of 100 μm, the size at which particles are often considered potentially damaging (see, for instance, Kerley, 2013). The exact mass threshold at which particles become dangerous to spacecraft

* Corresponding author.

E-mail address: althea.moorhead@nasa.gov (A.V. Moorhead).

¹ Readers can obtain up-to-date orbital parameters and close-approach data at <http://ssd.jpl.nasa.gov/sbdb.cgi?sstr=2013+A1>.

² <http://mars.jpl.nasa.gov/programmissions/missions/future/maven/>.

will depend on the spacecraft itself, its properties, and the impact speed (which will in this case be similar to the relative encounter speed of Siding Spring and Mars; i.e., 56 km/s). While we present results for particles 4.19×10^{-6} g or larger, the analytic model we present enables recalculation of the fluence for the desired particle mass range. This fluence can then be combined with satellite parameters to obtain a risk of impact.

Our algorithm is as follows:

1. We obtain or extrapolate the total brightness of the coma at the time of close encounter from current or past observations (Section 2.1).
2. We translate this brightness into a total dust surface area using the dust albedo (Section 2.2).
3. We translate dust surface area into dust number density via an assumed particle size distribution (Section 2.3).
4. We integrate along the spacecraft's trajectory through the coma to obtain the total fluence, assuming a spherically symmetric dust distribution (Section 2.4).

In order to model the coma dust environment, we rely on several observational studies, particularly data taken in the coma of 1P/Halley by the *Giotto* spacecraft's Dust Impact Detection System (DIDSY), presented by McDonnell et al. (1986) and further analyzed by Fulle et al. (2000). 1P/Halley is a Halley-type comet with a perihelion distance half that of Siding Spring; therefore, we limit our reliance on 1P/Halley to the general form of the dust size distribution and spatial distribution. We then supplement this with quantizations of dust physical properties (for instance, density) from other studies.

The *Giotto* spacecraft recorded numerous dust and meteoroid impacts along its route through the coma of 1P/Halley. Additionally, several post-*Giotto* missions have also recorded cometary dust and meteoroid impacts: *Deep Impact* recorded four particle impacts during its encounter with Tempel 1 (A'Hearn et al., 2008), and *Stardust* recorded numerous particle impacts during its passage through the comae of Tempel 1 (Economou et al., 2013) and Wild 2 (Tuzzolino et al., 2004). These mission data present an opportunity for validating our model. In Section 3.1 we reproduce the dust flux as a function of cometocentric distance measured by *Giotto* and in Section 3.2 we reproduce the number of observed dust impacts near Wild 2 as summarized by Tuzzolino et al. (2004).

After validating our model using comets Halley and Wild 2, we apply our model to Siding Spring to estimate the total meteoroid fluence at Mars during the comet's close encounter with that planet. The analytic approach described above allows us to estimate the particle fluence, to within an order of magnitude, without simulating the coma dynamics. This simplified method is desirable because it illustrates the dependence of the total fluence on observables and, most importantly, enables quick recalculation of the expected fluence as new observations are made.

We also pair this analytical approach with dynamical simulations of particles ejected from the nucleus of Siding Spring. The total number of particles simulated is essentially a free parameter and does not provide a check on the total fluence. Instead, these simulations illustrate the degree to which the coma of Siding Spring deviates from the perfect sphere described by our analytic model. We also use simulation results to determine the time and duration of the meteor shower the comet will produce at Mars.

2. Analytic model

In this section we describe our analytic, spherically symmetric cometary coma model, in which we relate the size and spatial

distribution of solids in the coma to comet brightness. We then derive an expression for the total dust or meteoroid fluence along a chord through the coma.

2.1. Cometary magnitude

The apparent magnitude of small bodies, including comets, follows the relation

$$m = M1 + 5 \log \Delta + 2.5n \log h, \quad (1)$$

where m is the apparent magnitude, $M1$ is the absolute magnitude, Δ is the distance, in au, between the object and the observer, and h is the heliocentric distance, also in au. The coefficient n parametrizes the dependence of comet brightness on heliocentric distance. Below, we relate the absolute magnitude to dust abundance in the coma.

First, we express the apparent magnitude relative to apparent solar magnitude at 1 au:

$$m - m_{\odot,1\text{au}} = -2.5 \log \frac{F_{c,h,\Delta}}{F_{\odot,1\text{au}}}. \quad (2)$$

$F_{c,h,\Delta}$ represents the light flux of the comet at the observer's location, while $F_{\odot,1\text{au}}$ is the light flux of the Sun at 1 au. At 1 au, the Sun has an apparent magnitude $m_{\odot,1\text{au}} = -26.74$.

The reflectivity of asteroids and comets is measured in terms of the geometric albedo, or reflectance at zero phase angle. This reflectance is expressed relative to the geometric albedo of a Lambertian disk – the intensity of light reflected by a perfectly diffusive Lambertian disk at zero phase angle is four times that of an isotropic reflector such as a metallic sphere (van de Hulst, 1981; Barbieri, 2007). Hence, the flux at zero phase angle for such an object is I_{tot}/π rather than $I_{\text{tot}}/4\pi$.

Because a comet's brightness is due to reflected solar light, we can express the flux as seen from zero phase angle as follows:

$$F_{c,h,\Delta} = \frac{F_{\odot,h}}{\pi \Delta^2} \cdot aA(h) = \frac{F_{\odot,1\text{au}}}{\pi \Delta^2 (h/1\text{au})^2} \cdot aA(h) \quad (3)$$

where a is the geometric albedo and $A(h)$ is the illuminated area, or total cross-section. A comet produces a coma in response to solar irradiation; as it nears the Sun, volatiles sublimate and accelerate dust particles away from the nucleus. As a result, the total dust cross section is a function of heliocentric distance. If we take an approach similar to that of Sanzovo et al. (1996) and assume $A(h) = A_0(h/1\text{au})^{-\beta}$, the above equation becomes

$$F_{c,h,\Delta} = \frac{F_{\odot,1\text{au}}}{\pi \Delta^2} \cdot aA_0(h/1\text{au})^{-(2+\beta)}. \quad (4)$$

Insertion of the above relation into Eq. (2) yields

$$m = m_{\odot,1\text{au}} + 5 \log \Delta + 2.5(2 + \beta) \log \left(\frac{h}{1\text{au}} \right) - 2.5 \times \log \left(\frac{a}{\pi} \cdot A_0 \right). \quad (5)$$

Noting that $n = 2 + \beta$, we thus recover the form of Eq. (1), where

$$M1 = m_{\odot,1\text{au}} - 2.5 \log \left(\frac{a}{\pi} \cdot A_0 \right), \quad (6)$$

and A_0 has units of au^2 .

The default value of n is 4 for comets (Green et al., 2001); this translates to $\beta \sim 2$, or that the illuminated area of a comet follows an inverse-square law – i.e., to first order, the production of coma material is proportional to the intensity of solar radiation incident on the comet.

Comet activity and dust production is usually constrained using the observable quantity $[af\rho]$,³ where a is albedo, f is filling factor,

³ $[Af\rho]$ is the more common notation, but we use a here in order to avoid confusion with our area parameter, A .

and ρ is cometocentric distance (A'Hearn et al., 1984). Efforts to measure $[af\rho]$ for Siding Spring are underway and would help constrain the quantity of particles in the coma; however, this quantity has yet to be measured. Thus, we rely on the more readily available total cometary magnitude to estimate particle abundance.

Note that we have assumed zero phase angle for our derivation; we make this choice for several reasons. First, while Siding Spring has not been observed at zero phase, the Sun-target-observer angle was 11.4° on the last used observation date (2013 October 18), falling within the $\lesssim 20^\circ$ range often characterized as a “low” phase angle (Meech et al., 2005; Joshi et al., 2010). Second, there is no standard phase correction for comets (Hosek et al., 2013) that we can employ, nor has one been measured for Siding Spring. Third, as Kelley et al. (2013) point out, this is complicated by the fact that large and small particles will scatter light differently. For these reasons, we do not incorporate phase into our model; however, if future observations constrain the phase dependence of Siding Spring's coma, this dependence could be incorporated into our model via a multiplicative factor in a manner similar to that of Kelley et al. (2013).

2.2. Cross-sectional area of solids

We now again rearrange Eq. (6) in order to determine the total cross section of coma particles:

$$A_0 = g \frac{\pi}{a} 10^{-0.4(M1-m_{\odot,1au})} \text{au}^2. \quad (7)$$

We have introduced a factor, g , to represent the fractional dust contribution to the comet's total brightness. We set this value to be unity for most of this analysis but retain g in our expressions. Fulle et al. (2000) found that for certain values of density and albedo, dust particles within *Giotto*'s range of sensitivity could account for the total brightness of the coma ($g \sim 1$), but for large dust material density ($\rho = 1 \text{ g/cc}$), $g \sim 0.5$ provided a better fit to the data. Technically, the above total area includes the nucleus, but the contribution of the nucleus to comet brightness and thus surface area is negligible and can be ignored for the purposes of this model.

2.3. Dust size distribution

We adopt a simple power law with exponent k for the size distribution function, f , (Fulle et al., 2000; Kelley et al., 2013),

$$f(s) = Cs^{-k}, \quad (8)$$

where s represents dust particle radius and C is a normalization parameter. Then, the total cross-sectional area, A_d , and total number, N_d , of particles in the coma can be expressed in terms of $f(s)$:

$$A_d = \pi \int_{s_{\min}}^{s_{\max}} s^2 f(s) ds \quad (9)$$

$$N_d = \int_{s_{\min}}^{s_{\max}} f(s) ds \quad (10)$$

Next, we equate Eqs. (7) and (9) to determine the constant C :

$$C = \frac{g}{ah^\beta} 10^{-0.4(M1-m_{\odot,1au})} \text{au}^2 \frac{3-k}{s_{\max}^{3-k} - s_{\min}^{3-k}}. \quad (11)$$

The coefficient of the particle size distribution function, C , enables calculation of the total number and total surface area of dust particles. In the next section, we combine it with a spatial distribution to calculate total fluence along a trajectory.

2.4. Particle fluence

In order to calculate the number density, v , of dust particles, we assume a constant outward flux of dust particles. Thus,

$$v(r) = Dr^{-2}. \quad (12)$$

One expects an inverse-square dependence on cometocentric distance, r , if the comet steadily emits particles with a constant ejection velocity distribution; in this case, the coma size is determined by ejection speed and the duration of the comet's period of activity. In actuality, ejection velocity will be a function of heliocentric distance (Whipple, 1951; Jones, 1995; Crifo and Rodionov, 1997) and ejection is by no means steady and isotropic. However, $v \propto r^{-2}$ is a reasonable first order approximation that fits comet observations (A'Hearn et al., 1984; Fulle et al., 2000).

We can determine the constant D by equating the volumetric integral of Eq. (10) to Eq. (12) and substituting Eqs. (11) and (12) for f and C :

$$D = C \frac{s_{\max}^{1-k} - s_{\min}^{1-k}}{4\pi r_c(1-k)}. \quad (13)$$

Here, $r_{\max} = r_c$ describes the radius of the coma. Determination of the coefficient of the spatial number density, D , also permits the calculation of flux or fluence.

We calculate the fluence of particles along a straight trajectory through the coma. We express this fluence, σ , in terms of impact parameter, or distance of closest approach, b :

$$\sigma(b) = \int_{x_1}^{x_2} v(\vec{x}) dx = 2D \int_0^{x_2} \frac{dx}{x^2 + b^2} = \frac{2D}{b} \cos^{-1} \left(\frac{b}{r_c} \right), \quad (14)$$

where v is the number density (see Eq. 12) and the parameters x_1 and x_2 are the endpoints of the integration path.

2.5. Parameters

In order to apply the above model to Siding Spring, we must adopt a number of physical parameters for the comet, many of which cannot be measured without a spacecraft mission (parameters are summarized in Table 1). The number of unmeasured parameters motivated the decision to develop an analytic model; as new observations are made and new models constructed, we can quickly obtain new up-to-date fluence estimates. In this section we discuss our nominal parameter choices and express the fluence in terms of comet and particle properties.

We have adopted the dust size distribution model of Fulle et al. (2000), which was developed using impact data obtained from the flight of *Giotto* through the coma of 1P/Halley. *Giotto* probed dust masses ranging from 7.71×10^{-9} to 31.0 g (Fulle et al., 2000). In the case of Siding Spring, we restrict our fluence calculations to dust particles for which $m > m_* = 4.19 \times 10^{-6} \text{ g}$ or larger (which corresponds to a radius of $215 \mu\text{m}$ for a density $\rho = 0.1 \text{ g/cc}$); above this threshold, particles pose a potential threat to spacecraft (McNamara et al., 2004). Thus, we replace the lower size limit in Eq. (13) with m_* . With these substitutions, and combining Eqs. (11), (13), and (14), we obtain the relation:

$$\sigma_* = \frac{gh^{-\beta}}{a} \left(\frac{2}{\pi} \right)^{\frac{2}{3}} \left(\frac{\rho}{3} \right)^{\frac{2}{3}} 10^{-0.4(M1-m_{\odot,1au})} \text{au}^2 \times \left(\frac{3-k}{1-k} \right) \left(\frac{m_{\max}^{(1-k)/3} - m_*^{(1-k)/3}}{m_{\max}^{(3-k)/3} - m_{\min}^{(3-k)/3}} \right) \times \frac{\cos^{-1}(b/r_c)}{br_c} \quad (15)$$

From the above equation we can see that the fluence of large particles has a simple dependence on most of our parameters; for instance, fluence is inversely proportional to particle albedo.

Table 1
Key orbital and physical parameters for Comet C/2013 A1 (Siding Spring), our default values, and sources.

Parameter	Symbol	Default value	Reference
Total magnitude	M1	5.2	JPL
Heliocentric distance	$h = q$	1.4 au	JPL
Radial dependence exponent	$\beta = n - 2$	2.4	JPL
Approach distance	b	131,000 km	JPL
Albedo	a	0.04	Fulle et al. (2000)
Density	ρ	0.1 g/cc	Fulle et al. (2000)
Dust contribution fraction	g	1	Fulle et al. (2000) and Kelley et al. (2013)
Size distribution exponent	k	2.6	Fulle et al. (2000)
Minimum dust mass	m_{\min}	7.71×10^{-9} g	Fulle et al. (2000)
Maximum dust mass	m_{\max}	31.0 g	Fulle et al. (2000)
Coma radius	r_c	Variable	NA

The dependence on the exponent, k , of the size distribution is more complex, as seen in Eq. (8). For large negative values of k , large particles dominate the dust contribution to coma brightness, and $\sigma_* \propto m_{\max}^{-2}$. For large positive values of k , we instead see $\sigma_* \propto (m_*/m_{\min})^{-k}$, which goes to zero as $k \rightarrow \infty$. We plot the behavior of σ_* relative to k for intermediate values in Fig. 1. The depicted range, $1 \leq k \leq 5$, encompasses all values over which the fluence is enhanced relative to the fluence for our nominal value of k (2.6, Fulle et al., 2000). This range includes size distribution indices corresponding to catastrophic fragmentation, $k = 4.3$, collisional cascade, $k = 3.49$, and collisionally relaxed, $k = 3.01$ (Jenniskens, 2006). It is also possible for the size index to fall short of or exceed this range. For instance, Kelley et al. (2013) find a much steeper size distribution for comet Hartley 2, with $4.7 \leq k \leq 6.6$, and Vaubaillon and Reach (2010) argue for a shallow particle size distribution ($k = 0.52$) in the coma of Schwassmann–Wachmann 3.

The k range depicted in Fig. 1 was chosen to cover the range over which $\sigma_* \gtrsim \sigma_*(k=2.6)$ this range includes not only the $k = 2.6$ value of Fulle et al. (2000) but also includes, for instance, the larger $k \sim 3.8$ value that Kelley et al. (2013) measure for Hartley 2. We note that the fluence has a maximum at $k = 3.27$, at which σ is enhanced by a factor of 2.5 relative to the fluence at our nominal choice of $k = 2.6$.

3. Results

3.1. 1P/Halley

While our goal is to quantify the risk that Siding Spring, a long-period, Oort cloud comet, poses to Martian spacecraft, Comet 1P/Halley is the only comet for which numerous impacts of large coma

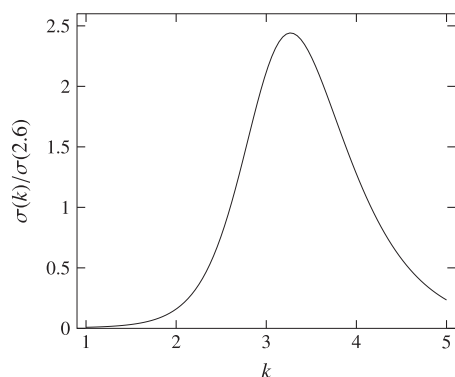


Fig. 1. Normalized fluence as a function of k . The fluence plotted is relative to the nominal value at $k = 2.6$, where k is the exponent of the dust size distribution. Note that variation in k can, at most, enhance the fluence by a factor of 2.5 relative to that obtained using our default value.

particles have been recorded. For this reason, we rely on models of 1P/Halley for particle properties.

For the same choice of albedo, dust size distribution, and density, the ratio of total number of particles in the coma of Siding Spring during the Mars encounter to the total number of particles in the coma of Halley during the *Giotto* encounter should be equal to the ratio of the total cross section of the particles. Using 3.88 for the absolute magnitude and 0.9024 au for the heliocentric distance of Halley's comet at the time of the *Giotto* flyby (Hughes, 1988), we obtain:

$$\frac{A_S}{A_H} = \frac{h_S^{2-0.4k_{1S}}}{h_H^{2-0.4k_{1H}}} \times 10^{-0.4(M_{1S}-M_{1H})} = 0.12 \quad (16)$$

We now apply our model to 1P/Halley to test for self-consistency, using Eqs. (12) and (13) to calculate the flux encountered by *Giotto* and comparing with observations. In its journey through Halley's coma, *Giotto* recorded thousands of dust impacts, with the first impact occurring at a cometocentric distance of 287,000 km and the last occurring at a distance of 202,000 km (McDonnell et al., 1986). The dust distribution was observed to be asymmetrical, but within 100,000 km Fulle et al. (2000) find that the dust abundance is inversely proportional to the square of the cometocentric distance, which is consistent with our simple model in Eq. (12).

Fig. 2 gives the dust flux, ζ , as a function of distance from the nucleus of 1P/Halley as recorded by *Giotto*'s dust impact detector (DID); we compare these data with the dust flux from our model:

$$\zeta(r) = v_C \cdot v(r), \quad (17)$$

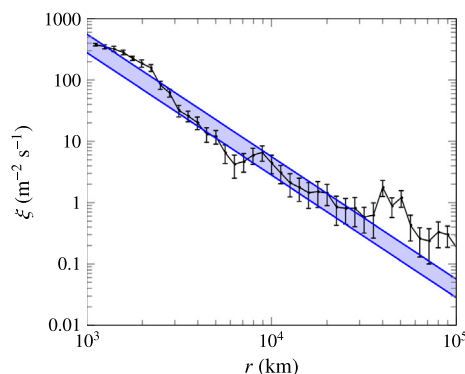


Fig. 2. Dust flux, ζ , as a function of cometocentric distance, r . Black data points and error bars are reproduced from Fulle et al., 2000. We calculate the expected dust flux using Eq. (17) and overlay it in blue on the *Giotto* data; the upper limit of the blue region represents flux values for a coma radius of 100,000 km, and the lower limit corresponds to a coma radius of 200,000 km. (For interpretation of the references to color in this figure legend, the reader is referred to the web version of this article.)

where $v_G = 68.4$ km/s is the velocity of the *Giotto* spacecraft relative to 1P/Halley (McDonnell, 1987). In calculating v , we use the same parameters as in Eq. (16), and assume a coma radius of $r_c = 100,000$ – $200,000$ km (Fulle et al., 2000; Xie and Mumma, 1996; Hodges, 1990).

While particles were detected at distances larger than 200,000 km, the distribution was observed to be asymmetrical and the relative error on the flux distribution at large radii is quite large. Thus, we consider our model to have successfully (i.e., within an order of magnitude) reproduced the dust flux encountered by *Giotto* near Halley. Note that in this case, we have calculated the total flux of all dust particles within the range 7.71×10^{-9} g– 31.0 g, while for Siding Spring we are interested in the flux of potentially hazardous large ($> 4 \times 10^{-6}$ g) particles.

3.2. 81P/Wild 2

On 2004 Jan 2, NASA's *Stardust* spacecraft flew within 300 km of Comet 81P/Wild 2, 98 days after the comet's perihelion passage. *Stardust* carried two dust impact sensors with different effective areas and multiple detection thresholds (see Table 2 of Tuzzolino et al., 2004). Although at most one particle larger than 4×10^{-6} g was detected by *Stardust*, we apply our coma model to Wild 2 and compare the fluence of smaller particles.

With a 2 km nuclear radius (Schmude, 2010), Wild 2 is significantly smaller than 1P/Halley, and at a heliocentric distance of 1.86 au during the *Stardust* encounter, much less active than Halley was during the *Giotto* encounter. Observations of Wild 2 shortly after its 1997 perihelion passage (Farnham and Schleicher, 2005) show a coma radius of 24,000 km at a heliocentric distance of 1.7 au. Schmude (2010) calculates an average absolute magnitude of 6.9 over several perihelion passages and a radial dependence parameter $\beta = 3.4$. We adopt these values for r_c , M1, and β and calculate the fluence for *Stardust*'s close approach distance of 236.4 km for each mass threshold; sensor properties including cross sectional area, mass thresholds, and number of impacts are listed in Table 2. We multiply these fluences by the relevant sensor surface area (Tuzzolino et al., 2004) and compare with the observed number of impacts (excluding the post-600 s spike in impacts); Fig. 3 compares the measured number of impacts with our predictions. We adjust the minimum mass of our particle distribution to match *Stardust*'s lowest detection threshold of 9.8×10^{-12} g; particles at the low end of the mass spectrum contribute very little to the total brightness and thus the resulting flux changes by a mere 3%, which is negligible compared to the effect of other properties such as coma radius and magnitude.

In contrast with *Giotto*'s 3 m² dust impact detector, *Stardust*'s 0.02 and 0.002 m² detectors are quite small. Additionally, Wild 2 has a smaller and less active coma than Halley. Nearly all particles detected by *Stardust* were smaller than 4×10^{-6} g; while our assumption of spherical symmetry is reasonable for large particles,

Table 2
Impact data from Tuzzolino et al., 2004 for both detectors on the *Stardust* spacecraft during its flyby of 81P/Wild 2.

Sensor	Channel	Mass threshold	Impacts before +600 s
Small (20 cm ²)	m1	9.8×10^{-12} g	1709
	m2	1.2×10^{-10} g	60
	m3	4.3×10^{-9} g	21
	m4	6.3×10^{-7} g	0
Large (200 cm ²)	M1	8.5×10^{-8} g	20
	M2	1.7×10^{-6} g	1
	M3	1.4×10^{-5} g	0
	M4	1.5×10^{-4} g	0

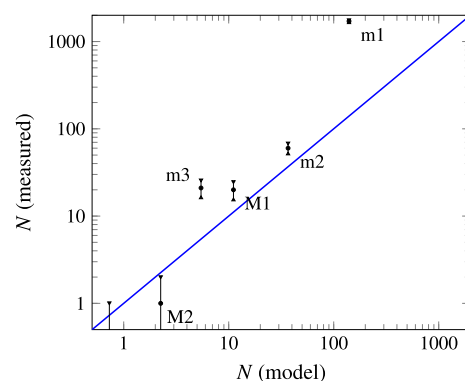


Fig. 3. Dust impacts recorded by the *Stardust* spacecraft near Wild 2. The number of impacts per sensor channel (see Table 2) recorded by *Stardust* during its flyby of 81P/Wild 2 is plotted against the number of impacts predicted by our analytic model. \sqrt{N} error bars are included, and the unity line is shown in blue for reference. (For interpretation of the references to color in this figure legend, the reader is referred to the web version of this article.)

such small particles are more subject to radiative forces and less likely to be symmetrically distributed around the nucleus. Images of the coma of Wild 2 after perihelion display less spherical symmetry than those occurring before perihelion (Farnham and Schleicher, 2005) and *Stardust* recorded short bursts of impacts, indicating that the spacecraft crossed through thin, dense sheets of ejecta (Sekanina and Chodas, 2012). In short, a sphere is a poor approximation to the shape of Wild 2's coma. To partially account for this, we have excluded a massive burst of small impacts recorded more than 600 s after close approach (see the rightmost column of Table 1 of Tuzzolino et al., 2004). We exclude these data because the existence of this burst indicates a high degree of spatial asymmetry for the smallest particles, which is not modeled by our spherical coma.

Despite these limitations, our model reproduces *Stardust* data to within an order of magnitude, with the exception of impacts in the m1 channel, which has the lowest mass detection threshold. It is possible to obtain closer agreement between *Stardust* data and our model by adjusting the particle size distribution (for instance, using a larger value of k), the particle bulk density (Tuzzolino et al., 2004 favor $\rho = 0.5$ g/cc), or the coma radius (if we assume the radius is smaller at 1.86 au than at 1.7 au). However, we have refrained from fitting six data points with as many parameters.

3.3. C/2013 A1 (Siding Spring)

Having verified our model using existing particle impact measurements for both Halley and Wild 2, we turn our attention to Siding Spring. While some of the comet's properties have been measured or constrained, including absolute magnitude and close approach distance, others, such as dust material density, are difficult to probe without a spacecraft mission. Additional coma properties may be measured later; for instance, measurement of $[af\rho]$ (albedo \times filling factor \times cometocentric distance, A'Hearn et al., 1984) would provide a useful probe of dust quantity and distribution.

In light of these uncertainties, we use available information for comet Siding Spring and supplement where necessary with typical physical cometary properties (Table 1). In Fig. 4, we investigate the variation of fluence with close approach distance and coma radius. The total number of particles in our model is determined by total cometary magnitude; therefore, a more compact coma results in a higher fluence but a smaller sphere of influence. Over all choices of coma radius, the maximum fluence of 4.19×10^{-6} g or larger particles at Siding Spring and Mars's close approach distance is

0.15 particles per square meter (Fig. 4). While this close approach distance is larger than the 100,000 km radius of Halley's coma, Siding Spring is a new, highly active Oort cloud comet and a large coma radius is likely. We adopt 0.15, which corresponds to a coma radius of approximately 200,000 km, as our nominal fluence in order to provide a rough idea of the possible risk posed to Martian spacecraft. We expect the coma radius to be measured or constrained as more detailed observations of the comet are made; for instance, the multi-aperture observations described in Hosek et al. (2013) could, if repeated for Siding Spring, constrain both $[af\rho]$ and coma radius. Once the radius has been better measured, an updated fluence can be obtained using Eq. (15).

As noted in our discussion of Eq. (15), this fluence may be enhanced or diminished if parameters differ from those in Table 1. This enhancement is bounded in one case – a different value of k can, at most, enlarge σ by a factor of 2.5 – but is in most cases unbounded. To illustrate these dependencies, we express the fluence at $b_{131} = 131,000$ km in terms of the values of physical parameters relative to their nominal values:

$$\sigma_*(b_{131}) \lesssim 0.15 \text{ m}^{-2} f_k g (1.4)^{-(\beta-2.4)} \left(\frac{a}{0.04}\right)^{-1} \times \left(\frac{\rho}{0.1 \text{ g/cc}}\right)^{\frac{2}{3}} 10^{-0.4(M1-5.2)}, \quad (18)$$

where $f_k = \sigma(k)/\sigma(k = 2.6) \leq 2.5$. Eq. (18) illustrates the mathematical dependence of the fluence on various physical parameters; in the next two sections, we discuss possible choices of these parameters.

3.3.1. Dust properties

Although a “typical” cometary albedo is about 0.04 (e.g., Fulle et al., 2000), much smaller values have been measured. For instance, Sekanina and Chodas (2012) determined the albedo of dust in the coma of Comet 17P/Holmes to be 0.006, and Fernández (2000) measured the albedo of fellow Oort cloud comet Hale-Bopp at 0.01. For the same magnitude, a lower albedo corresponds to a higher fluence. If, however, multiple reflections occur between particles in the coma, as suggested by Larson and A'Hearn (1984), the effective dust albedo could be higher, resulting in a low fluence despite a low true albedo.

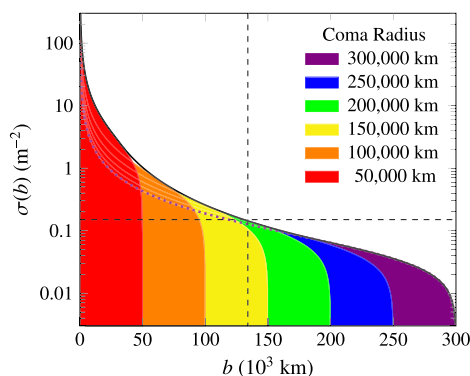


Fig. 4. Fluence as a function of close approach distance, b . Fluences for smaller coma radii are overlaid onto fluences for larger coma radii; i.e., red ($r_c = 5 \times 10^4$ km) on top of orange ($r_c = 10^5$ km). The solid black curve marks the maximum fluence at every value of b , obtained by varying r_c . The dotted purple curve depicts the fluence for our largest choice of coma radius, 300,000 km. The vertical dashed line marks the expected distance of closest approach between C/2013 A1 (Siding Spring) and Mars, which the JPL Small Body Database lists as 131,000 km as of 2013 October 21. The horizontal dashed line marks the fluence at this distance ($\sigma = 0.15$) given our choices of physical parameters, assuming a coma radius of $\sim 200,000$ km.

If the dust particles are simultaneously denser (say, $\rho = 1$ g/cc) and less reflective ($a = 0.01$), the fluence could be as large as a few particles per m^2 . However, models predict a correlation between albedo and density, with lower albedos occurring for more porous, less dense particles (Hage and Greenberg, 1990). If, as assumed by Fulle et al. (2000), ρ/a is a constant 2.5 g/cc, fluence will have a shallower dependence on density ($\sigma_* \propto \rho^{-1/3}$); in this case, a larger density actually produces a lower fluence. According to Fulle et al. (2000), at some point this constant ratio breaks down. They assert that a value $\rho = 1$ g/cc is not accompanied by a similarly large value of albedo and the dust cannot completely account for the brightness of the coma. We note that choosing $\rho = 1$ g/cc, $a = 0.04$, and $g = 0.5$ produces a 2.3-fold increase in fluence.

Kelley et al. (2013) also argue in favor of low density; *Deep Impact* detected significant numbers of large (≥ 1 cm) particles in the coma of 103P/Hartley 2 and the authors noted significant asymmetry in the spatial distribution of these particles. Kelley et al. (2013) argue that radiative forces are not capable of redistributing such large particles unless these particles have low density ($\rho \lesssim 0.1$ g/cc). Additionally, the same study argues in favor of a steep particle size distribution ($4.7 < k < 6.6$). According to Fig. 1, the adoption of a k value in this range results in a lower dust fluence in our model.

3.3.2. Cometary properties

The uncertainty in fluence due to dust properties pales in comparison to that resulting from uncertainty in the comet's orbit. For instance, Fig. 4 demonstrates that if the comet passes within a few thousand kilometers of Mars and its satellites, the result will be hundreds of impacts rather than 0.15 per square meter.

The magnitude may also deviate from the current estimate. Siding Spring is currently at a heliocentric distance of 4.7 au (according to JPL Horizons⁴ as of 2013 October 21). Thus, the current estimate for absolute cometary total magnitude, M1, is extrapolated from observations made early during the comet's approach. JPL Horizons cites an uncertainty of $M1 = 5.2 \pm 0.4$. Using Eq. (18), we determine that if the magnitude is at the brighter end of this range (i.e., $M1 = 4.8$), the dust abundance will increase by 50%.

The possible variation in fluence due to the combined effects of cometary properties and dust properties together spans orders of magnitude. In the next section, we perform numerical simulations in order to probe the true spatial distribution of the coma and the corresponding effect on fluence.

4. Numerical simulations

Our coma model assumes spherical symmetry, yet cometary comae are asymmetric (Schwarz et al., 1997, de Val-Borro et al., 2012, Vincent et al., 2013, Kelley et al., 2013, among others). In order to determine the degree to which Siding Spring's coma deviates from a sphere, we perform numerical simulations which take into account both gravitational effects and radiative forces. As the comet nears the Sun, it develops an extended tail in addition to a coma. However, this dust tail is not a distinct dynamical feature; there is a continuum between coma and tail in which the degree of spherical asymmetry depends on factors such as heliocentric distance and particle size. We take the entire dust component of the coma and tail continuum into account by simulating the ejection and evolution of dust particles from comet Siding Spring.

Our simulations include the eight planets with initial positions and velocities taken from the JPL DE405 ephemeris (Standish, 1998), with the Earth and Moon represented by a single particle at the Earth–Moon barycenter. The orbital elements for the comet

⁴ <http://ssd.jpl.nasa.gov/?horizons>.

Table 3

Orbital elements used in the simulation of Comet C2013A1 Siding Spring (J2000). These elements are for JD 2456320.5 (2013 January 28.0) when the comet was at a heliocentric distance of 7 au.

Element	Value
q (au)	1.39958
e	1.00036
i ($^\circ$)	129.0223
Ω ($^\circ$)	300.9648
ω ($^\circ$)	2.4307
τ_{peri}	2456956.05 (JD)
	2014 October 25 (TDB)

were taken from the JPL Small-Body Database on 2013 March 21 and are listed in Table 3. The system of planets, comet, and meteoroids were integrated with the RADAU method (Everhart, 1985) with a time step of 1 day used in all cases.

The comet was first observed on 2012 October 4 at a heliocentric distance of 7.2 au and was already active. This onset of activity well-beyond 3 au is characteristic of new Oort-cloud comets like Siding Spring (see, for example, for a summary Meech and Svoren, 2004). In order to capture any early activity, the position of the comet was initially integrated back in time 400 days to 25 December 2011 in order to place it at 10 au at the start of simulated activity. The comet was then integrated forward while producing

meteoroids according to the modified Whipple method (Brown and Jones, 1998), in which particles are ejected uniformly over the sunlit side of the comet, until its close encounter with Mars on 19 October 2014.

Particles with radii ranging from 10^{-5} to 10 cm (10^{-7} to 0.1 m) were simulated. Lacking more detailed information about the comet, some assumptions had to be made about the comet's properties. The comet nuclear Bond albedo was taken to be 0.05, the nuclear density to be 1 g/cc, the meteoroid density to be 0.1 g/cc, and the nuclear radius to be 1000 m. The simulation included the effects of radiation pressure. The ratio of solar radiation pressure to gravity, β_{rad} , is given by

$$\beta_{\text{rad}} = \frac{5.7 \times 10^{-5}}{\rho s}, \quad (19)$$

where ρ is density in g/cc and s is particle radius in cm (Burns et al., 1979; Weidenschilling and Jackson, 1993). The simulation can compute trajectories for particles on unbound orbits with respect to the Sun as well as for particles for which radiation pressure exceeds gravity (i.e., particles smaller than 5.7×10^{-4} cm for a density of 0.1 g/cc). In the latter case, $\beta_{\text{rad}} > 1$ and the particles are pushed out of the Solar System.

Simulation of the entire set of ejected particles, which number in the quadrillions, is prohibitively computationally expensive. Instead, we simulate the behavior of a representative number of particles and apply the following normalization factor:

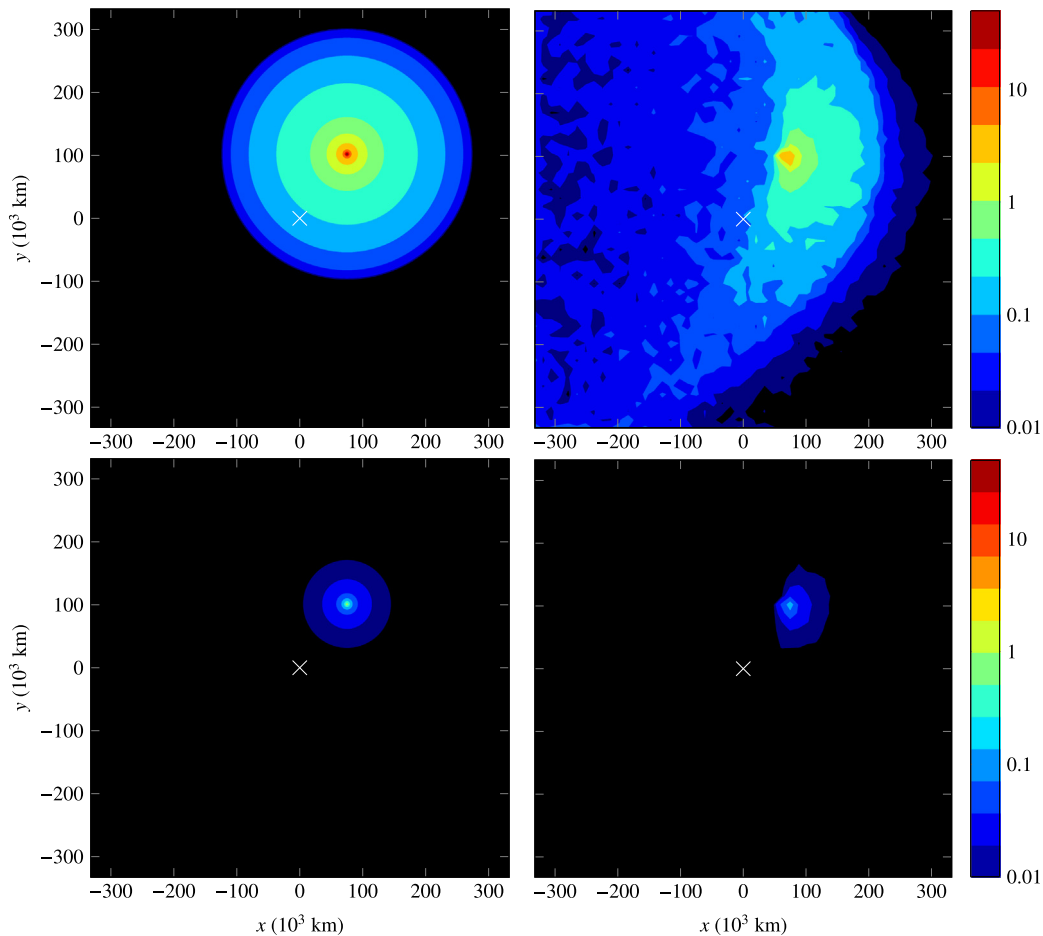


Fig. 5. Particle fluence maps at Mars due to Siding Spring. Predictions from our spherical model are on the left, and simulation results, renormalized to match the total number particles larger than 4.16×10^{-6} g (top) and 4.16×10^{-3} g (bottom) in this model, are on the right. Colors depict the total fluence per square meter as a function of location in a plane perpendicular to the velocity vector of C/2013 A1 (Siding Spring) relative to Mars. The planet Mars is located at the origin and marked with a white X. The y axis points toward Martian North and the x axis toward Martian East, which is the sunward direction.

$$\sigma_{\text{corr}} = \frac{N}{N_{\text{sim}}} = \frac{gh^{-\beta}}{aN_{\text{sim}}} 10^{-0.4(M_1 - m_{\text{oc},1\text{au}})} \times \left(\frac{3-k}{1-k} \right) \left(\frac{s_2^{1-k} - s_1^{1-k}}{s_{\text{max}}^{3-k} - s_{\text{min}}^{3-k}} \right) \quad (20)$$

where N_{sim} represents the total number of particles simulated between sizes s_1 and s_2 .

As the particles pass Mars, they are projected onto a target plane whose normal is defined by the comet's velocity relative to that planet. In Fig. 5, we compare model and simulation fluence results for two different mass regimes: $m > 4.19 \times 10^{-6}$ g (which corresponds to a grain radius of 215 μm at a density of 0.1 g/cc) and $m > 4.19 \times 10^{-3}$ g (which corresponds to 2.15 mm). The upward and right axes are taken to be Martian North and East respectively. The density of particles passing through the target plane yields the expected total fluence of particles in the planet's reference frame as the comet passes.

We can clearly see the effects of radiative forces on the particle distribution in Fig. 5, particularly in the top-right plot. Small particles are pushed anti-sunward (left, or Martian West, in our plots) and, as a result, sparsely fill a large region of space. Our analytic model does not include the extended coma, and thus underestimates the fluence at distances larger than our chosen coma radius. However, the fluence of 4.19×10^{-6} g or larger particles near Mars varies by a mere factor of 2 between the two maps.

The difference between our spherical model and the results of our simulations is less significant for large ($> 4.19 \times 10^{-3}$ g) particles; the primary difference is a slight flattening of the spatial distribution.

We find that the relative inaccuracy incurred by assuming spherical symmetry (roughly a factor of two near Mars) is small in comparison to orders-of-magnitude differences resulting from a change in close approach distance. We therefore recommend the use of our spherically symmetric analytic coma model for rapid re-estimation of the fluence near Mars as additional observations are made and comet properties are better measured or constrained. Using our nominal parameter values, our analytic model and numerical simulations both support an estimated impact probability of roughly 10–20% per square meter of spacecraft for 4.19×10^{-6} g particles.

Our numerical simulations yield additional information about the timing and duration of the meteor shower. We find that time of peak particle flux is nearly identical to the time of closest approach between Mars and Siding Spring, and that the bulk of the particle impacts will occur within an hour of the peak.

5. Conclusions

We have developed an analytic model of the dust abundance in cometary comae that can be used to obtain order-of-magnitude estimates of impact risk. This model relies on observables such as total cometary magnitude to estimate the brightness of the coma; this brightness is then combined with typical dust properties to generate a dust distribution. Finally, integration along a trajectory yields the total fluence of particles, which, for small fluences, is approximately the risk of impact.

This model can be applied to Comet C/2013 A1 (Siding Spring), which is projected to make a close approach to Mars on October 19, 2014. The close approach distance, 131,000 km, is sufficiently small that the comet is likely to engulf Mars and its natural and man-made satellites in the coma. We use the close approach distance and cometary magnitude to model the fluence of 4.19×10^{-6} g particles at Mars during the encounter. We find that while the exact number of expected impacts varies with comet and dust properties, our nominal value for the total fluence is 0.15 impacts per square meter.

We rely on studies of dust impact data recorded by the spacecraft *Giotto* on its route through Comet 1P/Halley's coma to constrain dust properties, but not dust quantity. To check for self-consistency, we model the coma of 1P/Halley itself and extract the fluence along *Giotto's* trajectory. We perform an additional check on our model by reproducing impact numbers as recorded by *Stardust* in the coma of Comet 81P/Wild 2. In both cases, our model agrees with the data at the order-of-magnitude level.

We check our assumptions regarding the spatial distribution (i.e., that it is spherically symmetric) by comparing our spherical model with simulations. These simulations produce an asymmetric coma and the fluence is reduced by a factor of 2 near Mars relative to our spherical model. We conclude that our analytic model sacrifices less than an order of magnitude in accuracy by neglecting particle dynamics and radiation pressure for particles larger than 4.19×10^{-6} g.

Comets are notoriously unpredictable; the magnitude of Siding Spring may very well change significantly as it moves inward through the Solar System. Additionally, neither the start of activity nor the size of the nucleus has been measured. Thus, we have expressed our results in parametrized form throughout this analysis, and our estimates can thus be easily updated as additional observations of C/2013 A1 (Siding Spring) are made.

Acknowledgments

This work was supported by NASA contract NNM12AA41C and NASA Cooperative Agreement NNX11AB76A. This work was also supported in part by the Natural Sciences and Engineering Research Council of Canada.

References

- A'Hearn, M.F., Schleicher, D.G., Millis, R.L., Feldman, P.D., Thompson, D.T., 1984. Comet Bowell 1980b. *Astron. J.* 89, 579–591, ISSN 0004-6256.
- A'Hearn, M.F. et al., 2008. Deep Impact and sample return. *Earth* 60, 61–66.
- Barbieri, C., 2007. *Fundamentals of Astronomy*. Taylor & Francis.
- Brown, P.G., Jones, J., 1998. Simulation of the formation and evolution of the Perseid meteoroid stream. *Icarus* 133 (1), 36–68.
- Burns, J.A., Lamy, P.L., Soter, S., 1979. Radiation forces on small particles in the Solar System. *Icarus* 40, 1–48.
- Crifo, J.F., Rodionov, A.V., 1997. The dependence of the circumnuclear coma structure on the properties of the nucleus. *Icarus* 129 (1), 72–93.
- de Val-Borro, M. et al., 2012. Submillimetric spectroscopic observations of volatiles in Comet C/2004 Q2 (Machholz). *Astron. Astrophys.* 545, A2–A14.
- Economou, T.E., Green, S.F., Brownlee, D.E., Clark, B.C., 2013. Dust flux monitor instrument measurements during stardust-NEXT flyby of Comet 9P/Tempel 1. *Icarus* 222 (2), 526–539.
- Everhart, E., 1985. An efficient integrator that uses Gauss–Radau spacings. In: Carusi, A., Valsecchi, G.B. (Eds.), *Dynamics of Comets: Their Origin and Evolution*. Reidel, Dordrecht, p. 185.
- Farnham, T.L., Schleicher, D.G., 2005. Physical and compositional studies of Comet 81P/Wild 2 at multiple apparitions. *Icarus* 173 (2), 533–558.
- Fernández, Y.R., 2000. The nucleus of comet Hale-Bopp (C/1995 O1): Size and activity. *Earth Moon Planets* 89 (1), 3–25.
- Fulle, M., Levasseur-Regourd, A.C., McBride, N., Hadamcik, E., 2000. In situ dust measurements from within the Coma of 1P/Halley: First-order approximation with a dust dynamical model. *Astron. J.* 119 (4), 1968–1977.
- Green, D.W.E., Marsden, B.G., Morris, C.S., 2001. Brightness predictions for comets. *Astron. Geophys.* 42 (1), 1.11–1.12.
- Hage, J.L., Greenberg, J.M., 1990. A model for the optical properties of porous grains. *Astrophys. J.* 361, 251–259.
- Hodges, R.R., 1990. Monte Carlo simulation of nonadiabatic expansion in cometary atmospheres – Halley. *Icarus* 83, 410–433.
- Hosek, M.W.J., Blaauw, R.C., Cooke, W.J., Suggs, R.M., 2013. Outburst dust production of Comet 29P/Schwassmann–Wachmann 1. *Astron. J.* 145 (5), 122–129.
- Hughes, D.W., 1988. The brightness of P/Halley and the surface activity of the nucleus at previous apparitions. *Mon. Not. R. Astron. Soc.*, 173–176, ISSN 0035-8711.
- Jenniskens, P., 2006. Meteor Showers and their Parent Comets. Meteor Showers and their Parent Comets.
- Jones, J., 1995. The ejection of meteoroids from comets. *Mon. Not. R. Astron. Soc.* 275 (3), 773–780.
- Joshi, U.C., Ganesh, S., Baliyan, K.S., 2010. Optical polarimetry and photometry of Comet 17P/Holmes. *Mon. Not. R. Astron. Soc.* 402 (4), 2744–2752.

- Kelley, M.S., Lindler, D.J., Bodewits, D., A'Hearn, M.F., Lisse, C.M., Kolokolova, L., Kissel, J., Hermalyn, B., 2013. A distribution of large particles in the coma of Comet 103P/Hartley 2. *Icarus* 222 (2), 634–652.
- Kerley, G.L., June 2013. Equation of State and Constitutive Models for Numerical Simulations of Dust Impacts on the Solar Probe.
- Larson, S.M., A'Hearn, M.F., 1984. Comet Bowell (1980b) – Measurement of the optical thickness of the coma and particle albedo from a stellar occultation. *Icarus* 58, 446–450.
- McDonnell, J.A.M., 1987. The Giotto dust impact detection system. *J. Phys. E – Scient. Instrum.* 20, 741–758, ISSN 0022-3735.
- McDonnell, J.A.M. et al., 1986. Dust density and mass distribution near Comet Halley from Giotto observations. *Nature* 321, 338–341.
- McDonnell, J.A.M. et al., 1987. The dust distribution within the inner coma of Comet P/Halley 1982i – Encounter by Giotto's impact detectors. *Astron. Astrophys.* 187, 719–741.
- McNamara, H., Jones, J., Kauffman, B., Suggs, R., Cooke, W.J., Smith, S., 2004. Meteoroid Engineering Model (MEM): A meteoroid model for the inner Solar System. *Earth Moon Planets* 95 (1), 123–139.
- McNaught, R.H., Sato, H., Williams, G.V., 2013. Comet C/2013 A1 (siding spring). *Cent. Bureau Electr. Telegrams* 3368, 1.
- Meech, K.J., Svoren, J., 2004. Using cometary activity to trace the physical and chemical evolution of cometary nuclei. *Comets II*, 317–335.
- Meech, K.J. et al., 2005. The Deep Impact Earth-based Campaign. *Space Sci. Rev.* 117 (1), 297–334.
- Sanzovo, G.C., Singh, P.D., Huebner, W.F., 1996. Dust colors, dust release rates, and dust-to-gas ratios in the comae of six comets. *Astron. Astrophys. Suppl.* 120, 301–311.
- Schmude, R.W., 2010. *Comets and How to Observe Them*. Springer.
- Schwarz, G., Cosmovici, C.B., Crippa, R., Guaita, C., Manzini, F., Oldani, V., 1997. Comet Hale-Bopp: Evolution of jets and shells during March 1997. *Earth Moon Planets* 78 (1), 189–195.
- Sekanina, Z., Chodas, P.W., 2012. Comet C/2011 W3 (Lovejoy): Orbit determination, outbursts, disintegration of nucleus, dust-tail morphology, and relationship to new cluster of bright sungrazers. *Astrophys. J.* 757 (2), 127–159.
- Standish, E.M., 1998. The JPL planetary and lunar ephemerides, DE405/LE405. JPL Interoffice Memorandum, 1–18.
- Tuzzolino, A.J. et al., 2004. Dust measurements in the coma of Comet 81P/Wild 2 by the dust flux monitor instrument. *Science* 304 (5), 1776–1780.
- van de Hulst, H.C., 1981. *Light Scattering by Small Particles*. Dover, New York, p. 112.
- Vaubailon, J.J., Reach, W.T., 2010. Spitzer space telescope observations and the particle size distribution of Comet 73P/Schwassmann–Wachmann 3. *Astron. J.* 139 (4), 1491–1498.
- Vincent, J.B., Lara, L.M., Tozzi, G.P., Lin, Z.Y., Sierks, H., 2013. Spin and activity of Comet 67P/Churyumov–Gerasimenko. *Astron. Astrophys.* 549, A121–A130.
- Weidenschilling, S.J., Jackson, A.A., 1993. Orbital resonances and Poynting–Robertson drag. *Icarus* 104, 244–254.
- Whipple, F.L., 1951. A comet model. II. Physical relations for comets and meteors. *Astrophys. J.* 113, 464–474.
- Xie, X., Mumma, M.J., 1996. Monte Carlo simulation of cometary atmospheres: Application to Comet P/Halley at the time of the Giotto spacecraft encounter. I. Isotropic model. *Astrophys. J.* 464, 442–446.